10-2012

Strain Rate and Orientation Dependencies of the Strength of Single Crystalline Copper under Compression

Virginie Dupont
Embry Riddle Aeronautical University, dupontv@erau.edu

Timothy C. Germann
Los Alamos National Laboratory

Strain rate and orientation dependencies of the strength of single crystalline copper under compression

Virginie Dupont* and Timothy C. Germann†
Los Alamos National Laboratory, Los Alamos, New Mexico 87545, USA
(Received 13 July 2012; published 15 October 2012)

Molecular dynamics (MD) simulations are used to model the compression under uniaxial strain of copper single crystals of different orientations at various temperatures and strain rates. Uniaxial strain is used because of the close resemblance of the resulting stress state with the one behind a shock front, while allowing a control of parameters such as strain rate and temperature to better understand the behavior under complex dynamic shock conditions. Our simulations show that for most orientations, the yield strength of the sample is increased with increasing strain rate. This yield strength is also dependent on the orientation of the sample, but less dependent on temperature. We find three regimes for the atomistic behavior around the yield: homogeneous dislocation nucleation, appearance of disordered atoms followed by dislocation nucleation, and amorphization. Finally, we show that a criterion solely based on a critical resolved shear and normal stress is insufficient at these strain rates to determine slip on a system.

DOI: 10.1103/PhysRevB.86.134111 PACS number(s): 62.20.fg, 31.15.xv, 62.50.−p

I. INTRODUCTION

The response of materials to high strain rate loading (above 10^6 s^{-1}) has long been of great interest because of its many industrial, transportation, and defense applications in shocks and impacts.[1] It is known that the yield stress of the material, defined as the shear stress reached before any dislocations are nucleated in the material, increases with increasing strain rate.[2–5] Experimentally, it is hard to get data at these high strain rates, not because they cannot be achieved, but because the measurement of strength at such high strain rates (and thus short time scales) is difficult.[6,7] Dynamic strength has been indirectly inferred from its role in inhibiting the growth of Rayleigh-Taylor[8–13] and Richtmyer-Meshkov[14] instabilities. A few impact and shock experiments have been exploring increasingly high strain rates,[3–5] and recently the strength of copper at a strain rate of 10^{10} s^{-1} has been measured.[15]

Molecular dynamics (MD) simulations offer the unique advantage that the conditions of the simulation can be controlled very precisely, and at the same time, the atomistic behavior of the material can be observed at any moment and at any location in the sample. Moreover, the strain rates usually obtained using MD simulations are comparable to those achieved in shock experiments (10^8 s^{-1} and above). Direct nonequilibrium MD (NEMD) shock simulations, however, require extensive computing time, because the samples must be sufficiently long for a steady shock wave to be established.[16–19] Techniques such as the moving window[20] can alleviate the problem of the number of atoms, but a good understanding of the dynamic strength of materials can also be reached by simulating the uniaxial compression of smaller samples. Another advantage of this approach is that the strain rate and temperature of the samples can be controlled, unlike in direct NEMD simulations.

MD simulations of single crystalline nickel under shear loading have shown that the yield stress increases with increasing strain rates, as a result of phonon drag.[21] Moreover, uniaxial tensile loading simulations showed that the yield strength is sensitive to boundary conditions, loading direction and applied strain rate.[22] Tschopp and McDowell[23] also studied the influence of the loading direction on the yield stress, and found that the study of the resolved shear stress on slip planes in both the slip direction (Schmid factor) and the normal direction (normal factor) are of importance to understand dislocation nucleation in single crystalline copper. In a study on single crystalline nickel nanowires under tension, Wen *et al.*[24] observe two critical strain rates (5×10^9 and 8×10^{10} s^{-1}) that play a pivotal role in switching between plastic deformation modes.

We present here MD simulations of the response of copper single crystals to uniaxial compression. We obtain measurements on the yield strength of these samples for four different orientations, three temperatures, and strain rates between 10^8 and 10^{11} s^{-1}. The paper is organized as follows. Section II describes the methods used in our simulations. In Sec. III, we analyze the results of compression along the [111],[110], and [123] directions. Sections IV and V describe the plastic deformations at yield and the transition to high strength for these orientations. In Sec. VI, we focus on the compression along the [001] direction, before concluding in Sec. VII.

II. METHODS

A. MD simulations

Molecular dynamics simulations of uniaxial shockless compression were conducted using the open source code LAMMPS.[25] A periodic cubic box of size $18 \times 18 \times 18$ nm^3 was created and filled with atoms in different crystallographic orientations: [001],[111],[110], and [123] along the compression axis ($\vec{z}$), resulting in systems of roughly 500 000 atoms. As suggested in Ref. 26, the box size was kept above 40 unit cells to avoid finite-size effects, especially in the [001] direction. Indeed, for box sizes smaller than that, phonon modes risk missing the unstable region within the Brillouin zone, hence artificially extending the elastic response of the material.[26] An embedded atom method potential[27] was used to represent the interactions between Cu atoms. The system was first relaxed with an energy minimization using the conjugate gradient method.[28] It was then thermalized in the isothermal-isobaric

ensemble (NPT) at zero pressure. Finally, the system was deformed in the canonical ensemble (NVT) by uniaxially compressing the simulation box at a constant engineering strain rate and rescaling atom positions according to the new box size.

The systems were held at constant temperatures of 50, 300, or 600 K using a Nosé-Hoover thermostat.[29,30] Strain rates ranging from 10^8 to 10^{11} s^{-1} were used to compress the box along the $\vec{z}$ direction (uniaxial strain loading). The time step of the simulations varied depending on the strain rate, ranging from 0.5 fs for the highest strain rate to 2 fs for the lowest one. Visualization of crystallographic defects is made possible through the use of the Ackland parameter.[31] In this paper, atoms in an fcc configuration are represented in grey, hcp (stacking faults) in blue, bcc in green, and all other atoms (dislocation cores, amorphous regions, and other defects) in red (color online).

B. Stress analysis

Stresses were calculated by averaging the virial stresses[32] over the entire system. These include both the kinetic and potential energy contributions. The deviatoric shear stress used in the rest of this paper is defined as

$$\tau = -0.5[\sigma_{33} - 0.5(\sigma_{11} + \sigma_{22})], \quad (1)$$

where σ_{33} is the normal stress in the compression direction.

In addition to stresses in this Cartesian (laboratory) reference frame, we also consider the resolved compression and shear stresses acting upon the available slip systems. We assume that the orientation of the slip planes at the yield point is very close to the initial orientation with respect to the compression axis, so that the initial orientation can be used in the following transformations. The rotation matrix (R) components are the cosines between the axes of the slip system (x_i') and the laboratory (x_i) frames of reference, such that

$$R_{ij} = \cos(x_i', x_j). \quad (2)$$

The stress transformation from the laboratory (σ) to the slip (σ') reference frame is then calculated using

$$\sigma' = R\sigma R^T. \quad (3)$$

The components of the new tensor include a shear stress corresponding to the critical resolved shear stress in simpler loadings (σ_{13}') if x_1' is the slip direction and x_3' is the slip normal, and the stress normal to the slip plane (σ_{33}').

III. COMPRESSION ALONG [111], [110], AND [123]

A. Yield stress analysis

Compression along these directions results in typical stress-strain curves (see Fig. 1), that exhibit an elastic rise, a maximum in stresses and a drop after the yield. The maximum shear stress is extracted and summarized in Fig. 2 for all three directions at 300 K. The effects of temperature are very small in comparison to the influence of strain rate or orientation, and are therefore not shown here. We notice that [123] and [110] have very similar yield stresses at low strain rates, with [110] having slightly higher yield stresses at high strain rates. Moreover, [111] has significantly higher yield stresses at low strain rates, but comparable yield stresses at high strain rates. In terms of strain, the [111] samples yield at a high strain compared to the other samples (between 16% and 20% for [111] compared to 10% to 17% for the other orientations). This extended elasticity compared to the other orientations makes the [111] samples stronger.

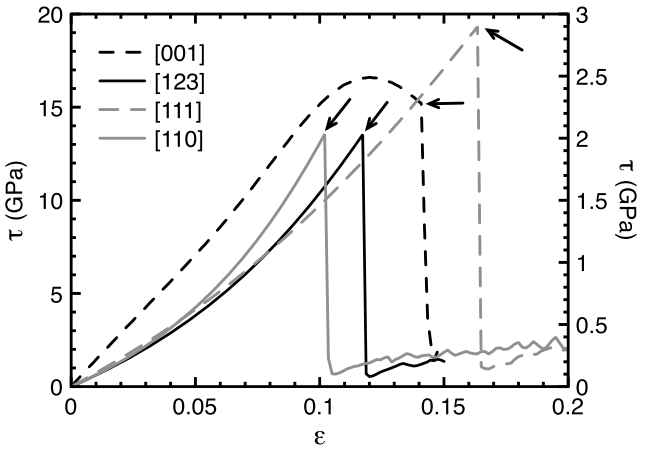

FIG. 1. Stress-strain curves for compression along the [123], [110], and [111] (left vertical scale), and [001] (right vertical scale) at 300 K and 10^8 s^{-1}. The strain threshold for dislocation nucleation is indicated with arrows.

Because of the complex stress state in the sample, a conventional Schmid factor and normal factor[23] analysis is impossible. We therefore conduct a full stress analysis on the 12 different slip systems that takes into account the measured stress state of our samples. We summarize in Table I the shear stresses on the slip systems for all three orientations at a strain rate of 10^8 s^{-1} at the yield point. The sample compressed along [111] exhibits the greatest amount of symmetry in its slip systems. One slip plane is normal to the loading direction and has thus almost zero shear stresses on all three directions, but the other three planes are virtually identical, each with two directions accumulating the same amount of stresses and the

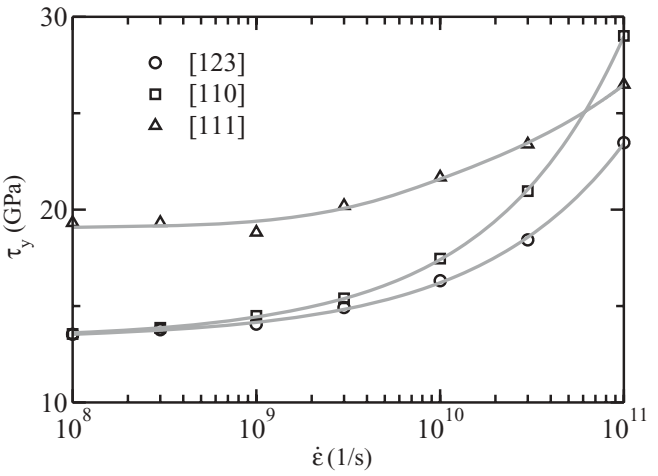

FIG. 2. Yield stress as a function of the strain rate for the [123] (circles), [110] (squares), and [111] (triangles) samples at 300 K. Fitted lines are provided as a guide to the eye.

TABLE I. Shear stresses on the different slip systems at the yield point for a strain rate of 10^8 s^{-1} at 300 K. The star indicates that this system is active at yield.

Slip plane	Slip direction	[123]	[111]	[110]
(111)	$[1\bar{1}0]$	−6.6877	−0.0025	−0.0009
	$[10\bar{1}]$	−8.9602	0.0019	9.7757
	$[01\bar{1}]$	−2.2724	0.0044	9.776*
$(\bar{1}11)$	[110]	10.991	10.5158	−0.0025
	[101]	10.4029*	10.5158	2.5678
	$[0\bar{1}1]$	−0.5884	0.0016	2.5695
$(1\bar{1}1)$	[110]	5.626	10.5103	−0.0018
	$[10\bar{1}]$	1.9107	−0.0045	−2.5686
	[011]	3.715	10.5148	2.5668
$(11\bar{1})$	$[1\bar{1}0]$	1.32	−0.0029	0.0009
	[101]	3.35	10.515	9.7749
	[011]	2.03	10.517*	9.774*

third direction having almost no shear stress. This means that no single slip system can yield before the other five available slip systems. For the other loading directions, there is no such obvious symmetry. In the case of the [123] compression, two slip systems have accumulated more shear stress and will thus yield first, while for the [110] compression, four slip systems show a comparable amount of shear. The symmetry in the case of the [111] compression means that six slip systems will yield at the same time, compared to only two and four in the other cases. Also, from this table, we see that at yield, the highest shear stresses are between 10 and 10.5 GPa for all compression directions. This indicates that the critical resolved shear stress (CRSS) is 10–10.5 GPa for copper. From Fig. 2, we see that a higher stress is required to achieve this CRSS in the sample compressed along the [111] direction at low strain rates.

To verify the results obtained from the stress analysis on the slip systems, we look at the atomic mechanisms in the samples around the yield point. We observe that at low strain rates, one or two systems are activated at yield (indicated by a star in Table I), but dislocations quickly cross slip onto other systems. Soon after the yield (within a few picoseconds), all four slip planes have at least one system active, regardless of the shear stress on the system. At higher strain rates, however, a reduced number of systems are activated for a good part of the simulation. For intermediate strain rates, a few systems are activated first, then slip propagates to other systems. The strain rate of the deformation is obviously a factor in these observations. In high strain rate simulations, dislocations do not have time to nucleate or propagate on all slip systems, unlike at low strain rates.

Tschopp and McDowell[23] have shown that not only the Schmid factor (giving the resolved shear stress on the slip plane) but also the normal factor (giving the resolved normal stress on the slip plane) were important in order to infer a yield criterion. They show that the critical stress for nucleation is the contribution of the resolved shear stress and the resolved normal stress, each contribution being weighted appropriately, meaning that for a small resolved shear stress, a large enough resolved normal stress could compensate and trigger slip. As shown in Table II, during the compression along [111], the normal stress on the (111) slip plane is much higher than normal stresses on any other plane, resulting in dislocation activity on this plane even though the shear stresses in all three slip directions are very small.

TABLE II. Normal stresses on the different slip planes at the yield point for a strain rate of 10^8 s^{-1} at 300 K.

Slip plane	[123]	[111]	[110]
(111)	39.716	68.769	30.735
$(\bar{1}11)$	30.332	34.424	10.583
$(1\bar{1}1)$	17.2518	34.425	10.58
$(11\bar{1})$	12.58	34.435	30.741

However, the normal stress on the (111) slip plane at 10^{11} s^{-1} reaches 104.2 GPa before dislocation activity occurs, a much higher stress than at lower strain rates. But since the resolved shear stress is zero, none of the slip systems in this plane are activated even at high strain rates, indicating that the threshold in the normal and shear stresses are not the only criteria for yield in the sample. Given the very high strain rates studied, the kinetics of dislocation nucleation is indisputably a factor, and because slip directions in the other three planes are activated at high strain rates for this sample, the time required for nucleation may be different on each slip plane, depending on its orientation with the compression axis.

B. Deformation microstructure following yield: Strain rate effects

Figure 3 shows snapshots of the deformation structures obtained after the yield point, once the stresses have decreased to a minimum, in all three samples for strain rates of 10^8, 3×10^9, and 10^{11} s^{-1} at 300 K. From the visualization of the samples, three regimes can be observed. In the first one (regime I), at low strain rate, yield is initiated by homogeneous dislocation nucleation. The first dislocation is nucleated at the highest stress, and is thus visible in the next image [see Figs. 3(a)–3(d)]. In the second regime (regime II), disordered atoms first appear in the sample, and dislocations are nucleated later. Dislocation nucleation in this case occurs after the yield point in the simulation for the sample compressed

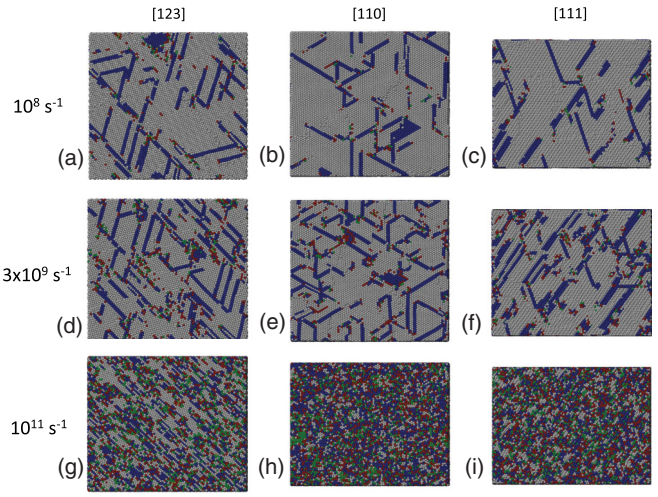

FIG. 3. (Color online) Crystallography of samples after the yield point for different strain rates. The compression axis on these snapshots is the vertical axis.

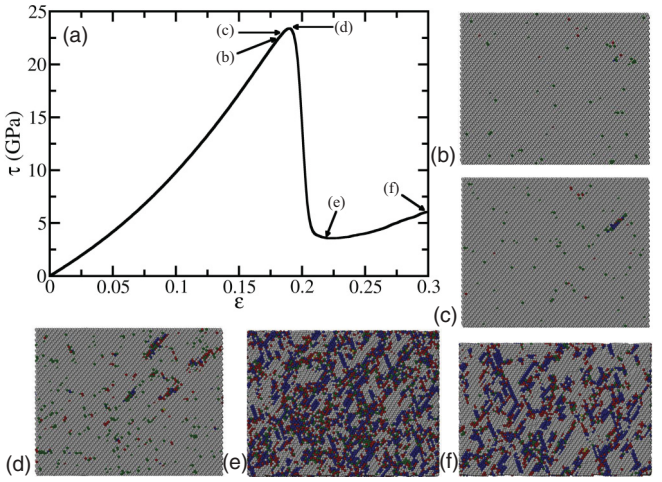

FIG. 4. (Color online) [111] sample deformed at 3×10^{10} s^{-1} and 300 K. (a) Stress-strain curve; (b) thermal noise just before the first nucleation; (c) first dislocation nucleation before stress maximum; (d) maximum shear stress, with more dislocations and disordered atoms; (e) stress minimum with numerous dislocations among disordered atoms; and (f) at 30% strain, dislocations have relaxed the sample and the disordered atoms are mostly gone.

along [110] [see Fig. 3(e)], and before the yield for the other two samples [see Fig. 3(f)]. The samples first show disordered atoms, and then dislocations are nucleated around those atoms. As dislocations relax the sample, the disordered atoms disappear. A sequence of events is presented in Fig. 4 for the case of a compression along the [111] axis at 300 K and a strain rate of 3×10^{10} s^{-1}. The transition between the first two regimes occurs between 3×10^{9} and 10^{10} s^{-1}. In the third regime (regime III), as opposed to the well-defined extended dislocations (red Shockley partial cores bounding blue stacking fault ribbons) that are generated at the lower strain rates [see Figs. 3(a)–3(f)], at the higher 10^{11} s^{-1} strain rate [see Figs. 3(g)–3(i)] the plastic deformation is caused by localized amorphous regions suggesting a crystal instability or virtual melting[33] rather than discrete dislocation slip activity. This is confirmed by the analysis of the percentage of atoms of each structure in the samples. At lower strain rates, most atoms are fcc (70–85%), some are in a stacking fault configuration (13–23%), and very few have another structure (2–7%). At high strain rates, however, the composition of the samples is very different, with less atoms in an fcc structure (22–40%), a similar number in an hcp configuration, this time representing both stacking faults and individual atoms having a local structure closest to hcp (27–35%), and more atoms do not fall in the previous two categories (32–43%). Although the percentage of fcc atoms is still high, it is important to note that the percentage of atoms being neither fcc or hcp increases by an order of magnitude. These samples are strained so rapidly that they reach the point of mechanical instability before deformation can localize by discrete dislocation slip. The transition between the last two regimes occurs around 10^{11} s^{-1}.

IV. COMPRESSION ALONG [001]

Uniaxial compression along the [001] orientation gives very unique results because of crystallographic reorientation

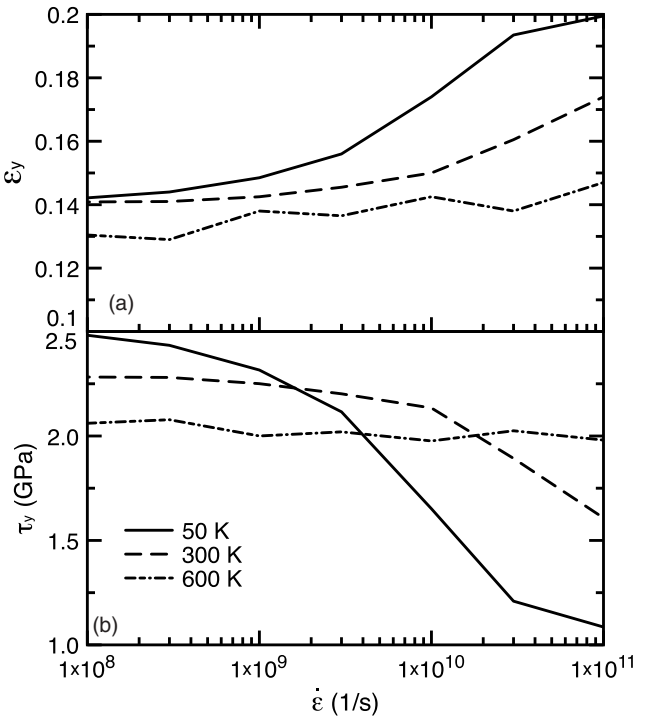

FIG. 5. Strain rate dependency of the (a) strain at the yield and (b) yield stress in a Cu sample uniaxially compressed along [001].

occurring along the Bain path,[34] which causes the fcc lattice to transform to a bcc lattice. As a result, the stresses reach a maximum and then elastically drop to zero as the transformation is finished at ∼29.3% compression. Because of this behavior, the maximum in the stress-strain curves does not necessarily represent the onset of plasticity. Instead, plasticity may not occur until after the maximum has been reached, on the side of the curve that decreases with increasing strain, as seen in Fig 1. It has been determined that for shock simulations, the nucleation of defects occurs only after a threshold strain has been reached, this threshold being 14% in Cu[26] and Lennard-Jonesium.[17,35] Moreover, because the portion of the curve where dislocations are nucleated is descending, as the strain rate increases, the overshoot in strain increases, as seen on Fig. 5(a). However, this results in a decrease in the yield stress and hence in a reversed trend compared to other orientations, as represented on Fig. 5(b). The amplitude of the drop in yield stresses (largest drop of 1.4 GPa at 50 K) is, however, very small compared to the amplitude of the increase with other orientations (the smallest increase being 7.2 GPa for [111] at 300 K).

The drop in the yield stress may be mostly attributed to the time required to nucleate dislocations, which is being overridden by the deformation time scale at higher strain rates. If we consider that yield happens around 14%,[26] the slower simulations will result in an almost instantaneous dislocation nucleation whereas the faster simulations will show some latency in terms of strain.

V. CONCLUSIONS

We have conducted MD simulations of compression under uniaxial strain of copper single crystals. Several orientations,

temperatures and strain rates were studied. For all orientations, we observe only a minor effect of the temperature, which was not studied in detail here.

We find that the orientation of the sample has a strong influence on the yield stress and its dependency on strain rate. In the case of compression along a [001] axis, the crystallographic rearrangement of atoms from fcc to bcc precludes any strengthening with increasing strain rate, as observed for the other orientations studied. The sample showing the most variation is the one compressed along the [110] direction, while the sample compressed along the [111] direction showed the least dependency. This sample is also the hardest at low strain rates and can accommodate larger strains for a wider range of strain rates, which is due to the high symmetry of its slip planes with regards to the compression direction.

We find that the deformations in the sample follow three regimes: (i) dislocation nucleation below $\sim 10^9$ to 10^{10} s^{-1}, (ii) disordered atoms followed by dislocation nucleation and relaxation of the sample, and (iii) little dislocation activity replaced by the creation of amorphous regions above $\sim 10^{11}$ s^{-1}. Dislocations are nucleated on all four slip planes at low strain rates, but on a reduced number of planes at higher strain rates. We also find that a criterion solely based on a stress threshold (even including normal stress on a slip plane) is not sufficient to determine the yield. The dynamics of dislocation nucleation has to be taken into account.

ACKNOWLEDGMENTS

We would like to thank R. Ravelo and B.L. Holian for valuable discussions. This work was supported by the Advanced Simulation and Computing Program and was carried out under the auspices of the National Nuclear Security Administration of the US Department of Energy at Los Alamos National Laboratory under Contract No. DE-AC52-06NA2-5396.

*Now Virginie Rollin at Embry-Riddle Aeronautical University; virginie.rollin@erau.edu

†tcg@lanl.gov

[1] M. A. Meyers, *Dynamic Behavior of Materials* (Wiley, New York, 1994).

[2] W. Lee and C. F. Lin, Mater. Sci. Eng. A **308**, 124 (2001).

[3] P. S. Follansbee and G. T. Gray III, Mater. Sci. Eng. A **138**, 23 (1991).

[4] W. Tong, R. J. Clifton, and S. Huang, J. Mech. Phys. Solids **40**, 1251 (1992).

[5] M. A. Meyers, F. Gregori, B. K. Kad, M. S. Schneider, D. H. Kalantar, B. A. Remington, G. Ravichandran, T. Boehly, and J. S. Wark, Acta Mater. **51**, 1211 (2003).

[6] T. J. Vogler and L. C. Chhabildas, Int. J. Impact Eng. **33**, 812 (2006).

[7] S. N. Luo, D. C. Swift, T. E. Tierney IV, D. L. Paisley, G. A. Kyrala, R. P. Johnson, A. A. Hauer, O. Tschauner, and P. D. Asimow, High Press. Res. **24**, 409 (2004).

[8] J. F. Barnes, P. J. Blewett, R. G. McQueen, K. A. Meyer, and D. Venable, J. Appl. Phys. **45**, 727 (1974).

[9] D. H. Kalantar, B. A. Remington, J. D. Colvin, K. O. Mikaelian, S. V. Weber, L. G. Wiley, J. S. Wark, A. Loveridge, A. M. Allen, A. A. Hauer, and M. A. Meyers, Phys. Plasmas **7**, 1999 (2000).

[10] B. A. Remington *et al.*, Met. Mat. Trans. A **35**, 2587 (2004).

[11] H.-S. Park, B. A. Remington, R. C. Becker, J. V. Bernier, R. M. Cavallo, K. T. Lorenz, S. M. Pollaine, S. T. Prisbrey, R. E. Rudd, and N. R. Barton, Phys. Plasmas **17**, 056314 (2010).

[12] H.-S. Park, K. T. Lorenz, R. M. Cavallo, S. M. Pollaine, S. T. Prisbrey, R. E. Rudd, R. C. Becker, J. V. Bernier, and B. A. Remington, Phys. Rev. Lett. **104**, 135504 (2010).

[13] R. E. Rudd, T. C. Germann, B. A. Remington, and J. S. Wark, MRS Bull. **35**, 999 (2010).

[14] G. Dimonte, G. Terrones, F. J. Cherne, T. C. Germann, V. Dupont, K. Kadau, W. T. Buttler, D. M. Oro, C. Morris, and D. L. Preston, Phys. Rev. Lett. **107**, 264502 (2011).

[15] W. J. Murphy *et al.*, J. Phys.: Condens. Matter **22**, 065404 (2010).

[16] B. L. Holian and P. S. Lomdahl, Science **26**, 2085 (1998).

[17] T. C. Germann, B. L. Holian, P. S. Lomdahl, and R. Ravelo, Phys. Rev. Lett. **84**, 5351 (2000).

[18] K. Kadau, T. C. Germann, P. S. Lomdahl, and B. L. Holian, Science **31**, 1681 (2002).

[19] E. M. Bringa, A. Caro, Y. Wang, M. Victoria, J. M. McNaney, B. A. Remington, R. F. Smith, B. R. Torralva, and H. Van Swygenhoven, Science **16**, 1838 (2005).

[20] V. V. Zhakhovskii, K. Nishihara, and S. I. Anisimov, JETP Lett. **66**, 99 (1997).

[21] M. F. Horstemeyer, M. I. Baskes, and S. J. Plimpton, Acta Mater. **49**, 4363 (2001).

[22] H. Gao, Y. Huang, and F. F. Abraham, J. Mech. Phys. Solids **49**, 2113 (2001).

[23] M. A. Tschopp and D. L. McDowell, J. Mech. Phys. Solids **56**, 1806 (2008).

[24] Y. H. Wen, Z. Z. Zhu, and R. Z. Zhu, Comput. Mater. Sci. **41**, 553 (2008).

[25] lammps.sandia.gov.

[26] G. Kimminau, P. Erhart, E. M. Bringa, B. Remington, and J. S. Wark, Phys. Rev. B **81**, 092102 (2010).

[27] Y. Mishin, M. J. Mehl, D. A. Papaconstantopoulos, A. F. Voter, and J. D. Kress, Phys. Rev. B **63**, 224106 (2001).

[28] M. R. Hestenes and E. Stiefel, J. Res. Nat. Bur. Stand. **49**, 409 (1952).

[29] S. Nosé, J. Chem. Phys. **81**, 511 (1984).

[30] W. G. Hoover, Phys. Rev. A **31**, 1695 (1985).

[31] G. J. Ackland and A. P. Jones, Phys. Rev. B **73**, 054104 (2006).

[32] E. T. Lilleodden, J. A. Zimmerman, S. M. Foiles, and W. D. Nix, J. Mech. Phys. Solids **51**, 901 (2003).

[33] V. I. Levitas and R. Ravelo, P. Natl. Acad. Sci. **109**, 13204 (2012).

[34] E. C. Bain and N. Y. Dunkirk, Trans. AIME **70**, 25 (1924).

[35] J.-B. Maillet, M. Mareschal, L. Soulard, R. Ravelo, P. S. Lomdahl, T. C. Germann, and B. L. Holian, Phys. Rev. E **63**, 016121 (2000).